iScience

Article

Inhibitory maturation and ocular dominance plasticity in mouse visual cortex require astrocyte CB1 receptors

Graphical abstract

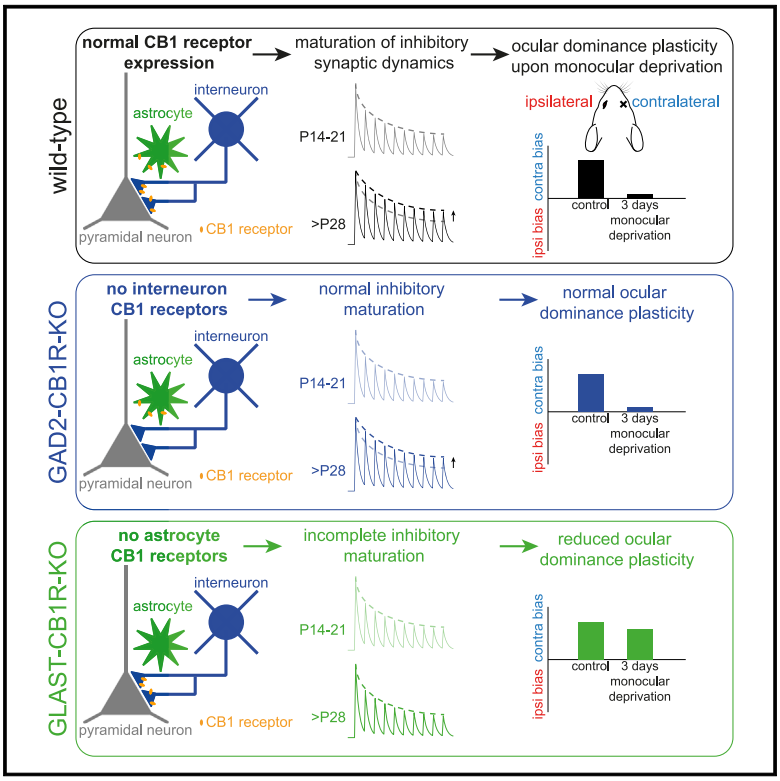

Highlights

- CB1 receptors on astrocytes are required for functional maturation in visual cortex
- Loss of CB1 receptors from interneurons does not affect inhibitory maturation
- Inactivation of astrocytic CB1 receptor disrupts ocular dominance plasticity

Authors

Rogier Min, Yi Qin, Sven Kerst, M. Hadi Saiepour, Mariska van Lier, Christiaan N. Levelt

Correspondence

r.min@amsterdamumc.nl (R.M.), c.levelt@nin.knaw.nl (C.N.L.)

In brief

Natural sciences; Biological sciences; Neuroscience; Systems neuroscience; Sensory neuroscience

Min et al., 2024, iScience *27*, 111410
December 20, 2024
https://doi.org/10.1016/j.isci.2024.111410

CellPress

iScience

CellPress
OPEN ACCESS

Article

Inhibitory maturation and ocular dominance plasticity in mouse visual cortex require astrocyte CB1 receptors

Rogier Min,[1,2,3,*] Yi Qin,[1] Sven Kerst,[1,2,3] M. Hadi Saiepour,[1] Mariska van Lier,[1] and Christiaan N. Levelt[1,4,5,*]

[1]Department of Molecular Visual Plasticity, Netherlands Institute for Neuroscience, an Institute of the Royal Netherlands Academy of Arts and Sciences, Amsterdam, the Netherlands

[2]Department of Child Neurology, Amsterdam Leukodystrophy Center, Emma Children's Hospital, Amsterdam University Medical Center, Amsterdam Neuroscience, Amsterdam, the Netherlands

[3]Department of Integrative Neurophysiology, Center for Neurogenomics and Cognitive Research, Vrije Universiteit Amsterdam, Amsterdam Neuroscience, Amsterdam, the Netherlands

[4]Department of Molecular and Cellular Neuroscience, Center for Neurogenomics and Cognitive Research, Vrije Universiteit Amsterdam, Amsterdam Neuroscience, Amsterdam, the Netherlands

[5]Lead contact

*Correspondence: r.min@amsterdamumc.nl (R.M.), c.levelt@nin.knaw.nl (C.N.L.)

https://doi.org/10.1016/j.isci.2024.111410

SUMMARY

Endocannabinoids, signaling through the cannabinoid CB1 receptor (CB1R), regulate several forms of neuronal plasticity. CB1Rs in the developing primary visual cortex (V1) play a key role in the maturation of inhibitory circuits. Although CB1Rs were originally thought to reside mainly on presynaptic axon terminals, several studies have highlighted an unexpected role for astrocytic CB1Rs in endocannabinoid mediated plasticity. Here, we investigate the impact of cell-type-specific removal of CB1Rs from interneurons or astrocytes on development of inhibitory synapses and network plasticity in mouse V1. We show that removing CB1Rs from astrocytes interferes with maturation of inhibitory synaptic transmission. In addition, it strongly reduces ocular dominance (OD) plasticity during the critical period. In contrast, removing interneuron CB1Rs leaves these processes intact. Our results reveal an unexpected role of astrocytic CB1Rs in critical period plasticity in V1 and highlight the involvement of glial cells in plasticity and synaptic maturation of sensory circuits.

INTRODUCTION

Neuronal circuits are shaped by experience. This happens much more readily in the young compared to the adult brain. The unique learning capacity of the young brain is regulated through postnatal critical periods, during which the ability of neuronal networks to re-wire is greatly enhanced.[1] Endocannabinoids, which signal through the cannabinoid CB1 receptor (CB1R), regulate several forms of neuronal plasticity.[2] In the developing neocortex, CB1Rs play a key role in the maturation of inhibitory circuits. In developing primary visual cortex (V1), endocannabinoid-mediated plasticity at inhibitory synapses regulates the maturation of inhibitory synaptic transmission, shifting synapses from an immature state characterized by strong short-term depression to a mature state with reduced short-term depression.[3,4] Additionally, immature inhibitory synapses can undergo an endocannabinoid-dependent form of long-term depression (iLTD), which is lost upon maturation. Completion of this inhibitory maturation correlates with the timing of the critical period for ocular dominance (OD) plasticity, which in mice peaks a P28-35[5] (with a similar but less well defined period in rats). In layer 2/3 (L2/3) of mouse V1, inhibitory maturation is complete at P28-30.[3] In rat V1, this maturation is complete approximately 1 week later.[4] Also in L5 of mouse V1, the timing of maturation and loss of iLTD is delayed by 1 week.[3] Rearing animals in the dark, which prolongs the critical period for OD plasticity,[6] delays the endocannabinoid-mediated maturation of inhibitory synaptic transmission.[4] This suggests that this maturation step contributes to critical period regulation in V1.

Although CB1Rs were originally thought to reside mainly on presynaptic axon terminals, several studies have highlighted an unexpected role for astrocytic CB1Rs in endocannabinoid mediated plasticity.[7–9] Here, we investigate the impact of cell-type-specific removal of CB1Rs from interneurons or astrocytes on development of inhibitory synapses and network plasticity of V1. We show that removing CB1Rs from astrocytes interferes with maturation of inhibitory synaptic transmission in V1. In addition, it strongly reduces OD plasticity during the critical period. In contrast, removing interneuron CB1Rs leaves these processes intact. Our results reveal an unexpected role of astrocytic CB1Rs in critical period plasticity in V1 and highlight the involvement of glial cells in the plasticity and synaptic maturation of sensory circuits.

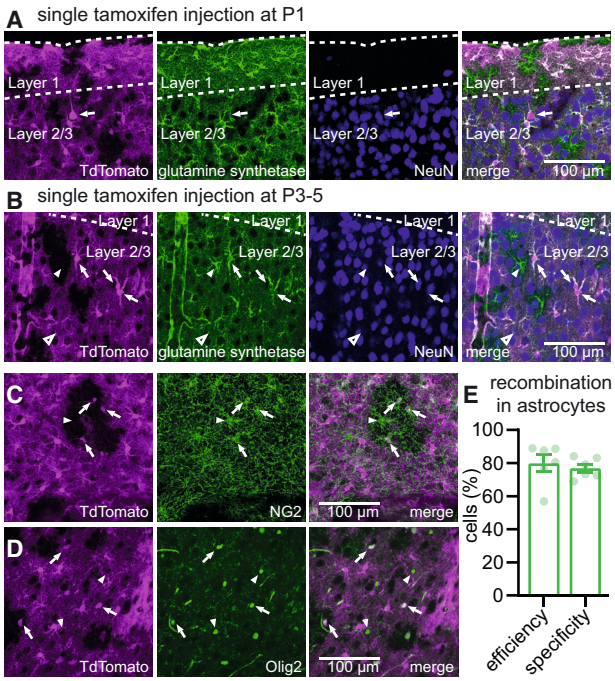

Figure 1. Early astrocytic recombination in GLAST-CreERT2 mice

(A) GLAST-CreERT2 TdTomato mice received a single i.p. injection of tamoxifen at P1. Slices containing V1 were prepared at P28-35, processed for immunofluorescence imaging and visualized using confocal microscopy. Recombination (indicated by TdTomato expression, magenta) was observed in astrocytes (visualized using a glutamine synthetase antibody, green) but also in sparse neurons (visualized using NeuN antibody, blue). An example neuron with pyramidal morphology is indicated by the arrow. Scale bar, 100 µm.

(B) Changing the tamoxifen injection regime to a single injection at P3-5 abolished neuronal recombination in V1, while astrocyte recombination was efficient (~80%). Arrows indicate TdTomato-expressing astrocytes, arrowheads indicate TdTomato-negative astrocytes.

(C and D) Specificity of recombination was high for astrocytes, but some non-neuronal recombination was seen in glial cells positive for NG2 (C, green, arrows) or Olig2 (D, green, arrows). Arrowheads indicate TdTomato-negative NG2-positive and Olig2-positive cells.

(E) Quantification of efficiency and specificity of recombination in astrocytes in mice receiving a single tamoxifen i.p. injection at P3-5, based on TdTomato and glutamine synthetase positivity ($N = 6$). Error bars indicate SEM.

RESULTS

Removal of astrocyte vs. interneuron CB1 receptors

CB1Rs are traditionally thought to reside on presynaptic axon terminals. However, the parvalbumin-expressing fast-spiking interneurons whose synapses undergo developmental maturation[4,10] are thought to express no or only low levels of CB1Rs.[11–13] Furthermore, it was previously shown that astrocytes also express CB1Rs,[7,8] which are involved in plasticity of developing sensory circuits.[8] To investigate how removal of CB1Rs from different cell types (astrocytes vs. interneurons) affects inhibitory maturation in V1, we made use of conditional knockout mice lacking CB1Rs in either astrocytes or interneurons. We crossed transgenic mice containing a floxed *Cnr1* gene (*Cnr1*$^{flox/flox}$ mice)[14] with different Cre-driver lines. For interneuron-specific recombination we used GAD2-Cre knock-in mice,[15] whereas for astrocyte-specific recombination we used GLAST-CreERT2 transgenic mice (JAX stock #012586).[16] The resulting mice lacked CB1Rs in either astrocytes ("GLAST-CB1R-KO mice") or interneurons ("GAD2-CB1R-KO mice").

Conditional recombination in GLAST-CreERT2 mice requires induction by tamoxifen injection. For our experiments, astrocyte-specific recombination needed to be induced at a young age, before the start of the critical period. A potential problem with early tamoxifen injection may be that recombination occurs in neuronal precursor cells, leading to recombination in neurons, as observed in another GLAST-CreRT2 mouse line.[17] We therefore tested at which age GLAST-CreERT2 induction was specific for glial cell types. Using a TdTomato Cre-reporter line crossed to GLAST-CreERT2 mice, we found that a single intraperitoneal (i.p.) tamoxifen injection at postnatal day 1 (P1) resulted in recombination in many glial cells, but also in a small number of neocortical neurons (Figure 1A). In contrast, a single injection between P3 and P5 resulted in efficient and specific recombination in glial cells, with no neuronal recombination in V1 observed throughout all cortical layers. Of all V1 astrocytes, 80% showed recombination, whereas 77% of recombined cells were astrocytes (Figures 1B–1E; $N = 6$), the rest being other glial cells (oligodendrocytes, oligodendrocyte precursor cells and NG2 cells; Figures 1C and 1D). This pattern of cortical recombination is identical to that observed in other studies utilizing the same GLAST-CreERT2 line combined with early postnatal tamoxifen injection: recombination almost exclusively in astrocytes, with less than 1% of recombined cells being Olig2 positive and negligible neuronal recombination.[18–20] Because astrocytes are the main glial cell type expressing CB1Rs (Allen Brain Atlas; www.brain-map.org), phenotypic changes observed in GLAST-CB1R-KO mice that are treated with tamoxifen at P3-5 are most likely due to loss of CB1R expression in astrocytes.

Loss of astrocytic CB1Rs interferes with inhibitory synaptic maturation

To investigate how loss of CB1Rs from specific cell types affected inhibitory synaptic maturation, we assessed short-term dynamics of inhibitory synapses in acute brain slices of P28-35 mice. Whole-cell patch-clamp recordings were made from L2/3 pyramidal neurons, and evoked inhibitory postsynaptic currents (IPSCs) were measured upon repetitive extracellular stimulation (10 pulses at 25 Hz; see methods for recording details). V1 inhibitory synapses onto L2/3 pyramidal neurons normally mature toward a state characterized by less pronounced short-term synaptic depression at P28-35, while inhibitory synapses in full CB1R knockout mice retain immature synaptic dynamics.[3,4] In our hands, the steady-state IPSC amplitude observed after stimulation with a train of stimuli slightly differed from that observed in earlier studies.[3,4] This is likely due to variations in recording settings and experimental details between labs. Importantly, we found that short-term dynamics of inhibitory synapses in P28-35 GAD2-CB1R-KO mice did not differ from that in wild-type littermates (Figure 2A; normalized steady state IPSC amplitude: wild-type: 0.42 ± 0.05, $n = 16/N = 5$; GAD2-CB1R-KO: 0.45 ± 0.05, $n = 19/N = 4$; $p = 0.71$; Mann-Whitney test), suggesting normal inhibitory maturation in the absence of interneuron CB1Rs. In contrast, GLAST-CB1R-KO mice showed more pronounced short-term depression when

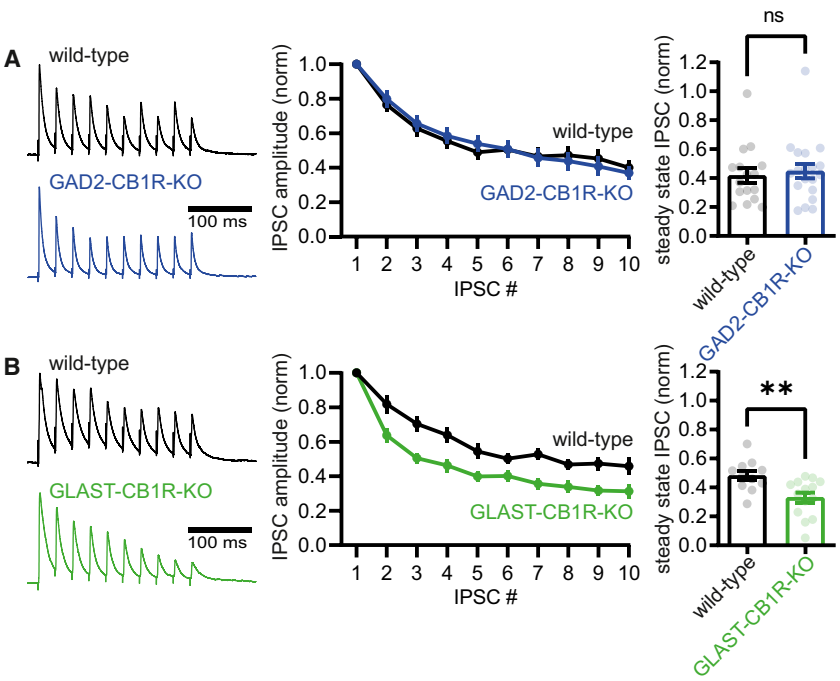

Figure 2. Impaired inhibitory synaptic maturation upon loss of astrocyte CB1 receptors

(A) Left: example traces showing the dynamics of inhibitory synaptic transmission in acute brain slices from GAD2-CB1R-KO mice (blue) and their wild-type littermates (black). Middle: averaged IPSC amplitude normalized to the first, for each of the 10 IPSCs in the train. Right: steady-state IPSC amplitude (averaged normalized amplitude of the last three IPSCs in the train) for all individual recorded neurons (dots). Bars show mean.

(B) Same as in (A) but for GLAST-CB1R-KO mice (green) and their wild-type littermates (black). Error bars indicate SEM. $^{*}p \leq 0.05$; $^{**}p \leq 0.01$; $^{***}p \leq 0.001$.

compared to wild-type littermates (Figure 2B; normalized steady state IPSC amplitude: wild-type: 0.48 ± 0.03, $n = 11/N = 4$; GLAST-CB1R-KO: 0.33 ± 0.03, $n = 14/N = 4$; $p = 0.008$; Mann-Whitney test). This suggests that loss of CB1Rs on astrocytes, but not on interneurons, interferes with the maturation of inhibitory synaptic transmission.

Long-term depression of inhibitory synapses is intact upon removal of interneuron or astrocyte CB1Rs

Inhibitory synapses in V1 can undergo endocannabinoid-mediated long-term depression (iLTD) at early developmental stages, but this form of plasticity is lost during maturation. iLTD is blocked by CB1R antagonists and absent in full CB1R knockout mice.[3,4] The significance of iLTD for inhibitory circuit functioning and maturation is unknown. To investigate how iLTD was effected by cell-type-specific CB1R removal, we prepared acute brain slices from young mice (P14-21) and performed whole-cell patch-clamp recordings from L2/3 pyramidal neurons. IPSCs were evoked by extracellular stimulation in L4, which likely recruits axons of local inhibitory interneurons that impinge onto L2/3 pyramidal neurons, including a large contribution by PV-positive fast-spiking interneurons.[4] Theta-burst stimulation of these synapses induces iLTD. To assess iLTD, evoked IPSCs were recorded for a baseline period of 10 min, followed by iLTD induction using a theta-burst protocol (see methods for additional details). In wild-type mice, this led to a significant reduction in IPSC amplitude, indicating robust iLTD expression (iLTD: 17.0 ± 2.9%, $n = 29/N = 17$, IPSC amplitude baseline vs. after iLTD induction: $p = 0.0002$, paired t test; Figure 3A). iLTD was abolished in the presence of the CB1R antagonist AM251 (10 μM; iLTD: 0.0 ± 4.2% iLTD, $n = 12/N = 6$, IPSC amplitude baseline vs. after iLTD induction: $p = 0.92$; % iLTD control vs. +AM251: $p = 0.002$, unpaired t test; Figure 3A).

Next, we investigated how iLTD was influenced by cell-type-specific removal of CB1Rs. Surprisingly, we found that removal of neither interneuron CB1Rs nor astrocyte CB1Rs affected the magnitude of iLTD (Figures 3B and 3C). iLTD did not significantly differ between interneuron CB1R knockouts and wild-type littermates (GAD2-CB1R-KO iLTD: 17.7 ± 3.7%, $n = 37/N = 16$, IPSC amplitude baseline vs. after iLTD induction: $p = 0.0002$, paired t test; wild-type littermates iLTD: 15.3 ± 3.6% iLTD, $n = 40/N = 15$, IPSC amplitude baseline vs. after iLTD induction: $p < 0.0001$; % iLTD wild-type vs. GAD2-CB1R-KO: $p = 0.65$, unpaired t test; Figure 3B). The same was true for astrocyte CB1R knockouts (GLAST-CB1R-KO iLTD: 11.1 ± 2.3%, $n = 44/N = 16$, IPSC amplitude baseline vs. after iLTD induction: $p < 0.0001$, paired t test; wild-type littermates iLTD: 10.7 ± 1.9% iLTD, $n = 37/N = 15$, IPSC amplitude baseline vs. after iLTD induction: $p < 0.0001$; % iLTD wild-type vs. GLAST-CB1R-KO: $p = 0.91$, unpaired t test; Figure 3C). Finally, we did not observe significant differences in the amount of iLTD in the three different control groups shown in Figures 3A–3C (wild-type controls, wild-type littermates of GAD2-CB1-KO mice, and wild-type littermates of GLAST-CB1-KO mice). Therefore, although inhibitory synaptic maturation relies on astrocyte CB1Rs, iLTD is surprisingly intact upon conditional removal of either astrocyte or interneuron CB1Rs. Similar results were obtained when we studied the effect of application of the synthetic CB1R agonist WIN55,212-2 on IPSC amplitude: a similar reduction in IPSC amplitude was observed in both astrocyte and interneuron CB1R knockouts (Figure S1).

Loss of astrocytic CB1Rs disrupts OD plasticity

The maturation of inhibitory synaptic transmission is known to be critical for the occurrence of OD plasticity during the critical period.[1] Therefore, we assessed OD plasticity in mice in which CB1R expression was disrupted in astrocytes or interneurons. Using optical imaging of intrinsic signal,[21] we measured responses to stimulation of the two eyes in the binocular region of V1, calculated the OD index (ODI; see methods), and compared mice that were reared normally (non-deprived) with mice that were monocularly deprived for 3 days starting around P28 (3 days MD). In wild-type

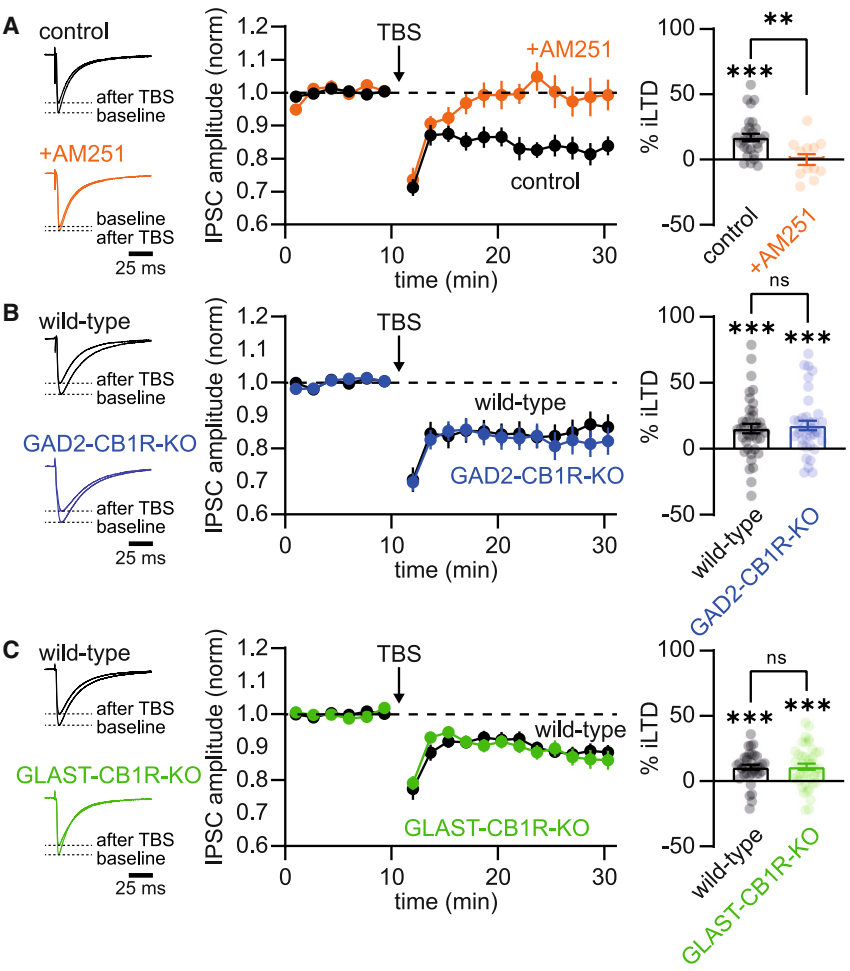

Figure 3. iLTD is unaffected by removal of astrocyte or interneuron CB1 receptors

(A) Left: example traces showing the averaged IPSC during the 10 min of baseline recording and 10–20 min after iLTD induction by TBS. Black traces are from a control experiment and orange in the presence of the CB1 receptor antagonist AM251. Middle: averaged time course of the IPSC amplitude normalized to baseline for all experiments under control conditions (black) and in the presence of AM251 (orange). Right: averaged amount of iLTD (% reduction of the IPSC amplitude after TBS) for all individual recorded neurons (dots). Bars show mean. (B) Same as in (A) but now for GAD2-CB1R-KO mice (blue) and their wild-type littermates (black).

(C) Same as in (A) and (B) but now for GLAST-CB1R-KO mice (green) and their wild-type littermates (black). Error bars indicate SEM. $^{*}p \leq 0.05$; $^{**}p \leq 0.01$; $^{***}p \leq 0.001$.

littermates of both GAD2-CB1R-KO and GLAST-CB1R mice, 3 days MD led to an OD shift (GAD2-CBR1-KO littermates: ODI non-deprived: 0.34 ± 0.04, $N = 5$; 3 days MD: 0.07 ± 0.05, $N = 6$; GLAST-CB1R littermates: ODI non-deprived: 0.33 ± 0.04, $N = 6$; 3 days MD 0.02 ± 0.06, $N = 7$; Figures 4A and 4B). This OD shift was also observed upon interneuron-specific CB1R removal (GAD2-CB1R-KO: ODI non-deprived: 0.31 ± 0.04, $N = 5$; 3 days MD: 0.03 ± 0.05, $N = 5$; Figure 4A). Statistical analysis yielded no interaction between genotype and molecular deprivation for GAD2-CB1R-KO mice (two-way ANOVA; interaction of genotype with OD shift $p = 0.93$; Tukey's post-hoc test: wild-type non-deprived vs. 3 days MD: $p = 0.002$; GAD2-CB1R-KO non-deprived vs. 3 days MD: $p = 0.003$; wild-type 3 days MD vs. GAD2-CB1R-KO 3 days MD: $p = 0.95$). In contrast, no significant OD shift was observed upon removal of astrocyte CB1Rs (GLAST-CB1R-KO: ODI non-deprived: 0.31 ± 0.04, $N = 7$; 3 days MD: 0.22 ± 0.04, $N = 8$; two-way ANOVA; interaction of genotype with OD shift $p = 0.022$; Tukey's post-hoc test: wild-type non-deprived vs. 3 days MD: $p = 0.0006$; GLAST-CB1R-KO non-deprived vs. 3 days MD: $p = 0.54$; wild-type 3 days MD vs. GLAST-CB1R-KO 3 days MD: $p = 0.021$; Figure 4B). Therefore, CB1Rs on astrocytes, not on interneurons, are required for OD plasticity during the critical period.

OD plasticity is disrupted in deeper cortical layers upon loss of astrocytic CB1Rs

OD plasticity measured using optical imaging of intrinsic signal likely mainly reports plasticity in superficial cortical layers.[22,23] Previous studies that described effects of pharmacological CB1R blockade on OD plasticity revealed that the effect of acute CB1R blockade on OD plasticity is layer specific, with OD plasticity in layer 2/3 of V1 being sensitive to treatment with a CB1R antagonist, whereas deeper layers show normal OD plasticity upon CB1R antagonist treatment.[24,25] To investigate whether the disruption of OD plasticity upon developmental loss of astrocytic CB1Rs was observed in deeper layers, we performed electrophysiological recordings using laminar probes in GLAST-CB1R-KO mice. Analyzing OD plasticity over all cortical layers confirmed the disruption of OD plasticity that we observed using intrinsic signal optical imaging. Upon removal of astrocyte CB1Rs, OD plasticity was still observed, but in significantly reduced form (wild-type: ODI non-deprived: 0.32 ± 0.03, $n = 162/N = 11$; 3 days MD: −0.04 ± 0.03, $n = 104/N = 7$; GLAST-CB1R-KO: non-deprived: 0.31 ± 0.03, $n = 139/N = 10$; 3 days MD: 0.15 ± 0.03, $n = 121/N = 8$; two-way ANOVA; interaction of genotype with OD shift $p = 0.002$; Tukey's post-hoc test: wild-type non-deprived vs. 3 days MD: $p < 0.0001$; GLAST-CB1R-KO non-deprived vs. 3 days MD: $p = 0.0006$; wild-type 3 days MD vs. GLAST-CB1R-KO 3 days MD: $p < 0.0001$; Figure 4C). Next, we specifically looked at OD plasticity in deeper cortical layers, by separately analyzing units in layer 4 and layer 5/6, based on depth. We found that loss of astrocytic CB1Rs reduced OD plasticity in deeper cortical layers (Figure 4D; L4: wild-type: ODI non-deprived: 0.32 ± 0.06, $n = 33/N = 11$; 3 days MD: −0.06 ± 0.06, $n = 21/N = 7$; GLAST-CB1R-KO: non-deprived: 0.25 ± 0.07, $n = 30/N = 10$; 3 days MD: 0.14 ± 0.05, $n = 24/N = 8$; two-way ANOVA;

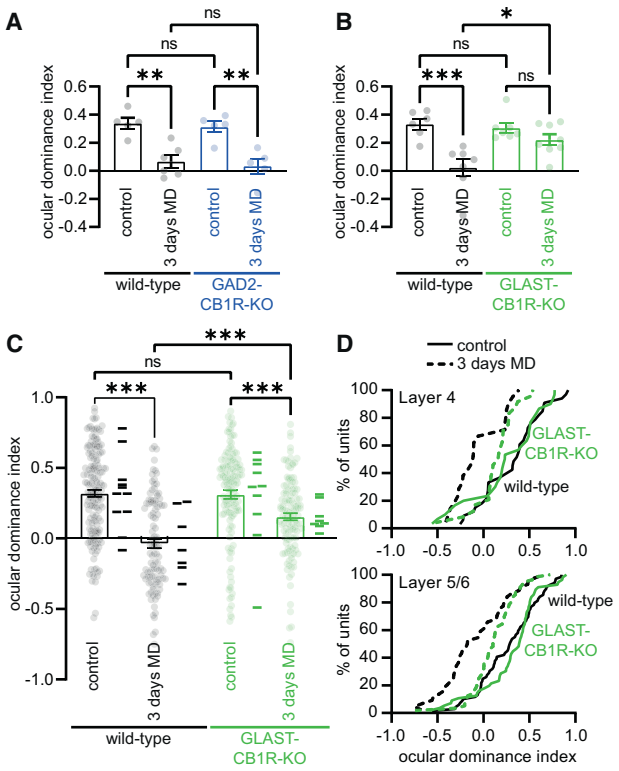

Figure 4. Ocular dominance plasticity is disrupted upon loss of astrocyte CB1 receptors

(A) Summary graphs of the ocular dominance index, as assessed using optical imaging of the intrinsic signal. Data are shown for GAD2-CB1R-KO mice (blue) and their wild-type littermates (black), both under control conditions and after 3 days of monocular deprivation (3 days MD). Dots indicate recorded ocular dominance index for individual mice. Bars show mean.

(B) Same as in (A) but now for GLAST-CB1R-KO mice (green) and their wild-type littermates (black).

(C) Same as in (A) and (B), but here ocular dominance index was assessed using *in vivo* electrophysiology. Dots represent individual single units, bars show mean, and lines next to the bars indicate averaged ocular dominance index for all units per mouse.

(D) Cumulative distribution of ocular dominance index against % of units, for deep cortical layers (L4 and L5/6). Dotted lines represent non-deprived controls, and solid lines represent 3 days monocular deprivation. Green lines show data from GLAST-CB1R-KO mice and black lines from wild-type littermates. Error bars indicate SEM. $^{*}p \leq 0.05$; $^{**}p \leq 0.01$; $^{***}p \leq 0.001$.

interaction of genotype with OD shift $p = 0.033$; L5/6: wild-type: ODI non-deprived: 0.28 ± 0.04, $n = 69/N = 11$; 3 days MD: −0.09 ± 0.05, $n = 44/N = 7$; GLAST-CB1R-KO: non-deprived: 0.31 ± 0.04, $n = 56/N = 10$; 3 days MD: 0.11 ± 0.03, $n = 56/N = 8$; two-way ANOVA; interaction of genotype with OD shift $p = 0.048$). Therefore, genetic removal of astrocytic CB1Rs during development has a different and broader effect on OD plasticity than acute pharmacological CB1R blockade.

DISCUSSION

In this study, we show that astrocytic CB1Rs contribute to the maturation of inhibitory synapses and affect OD plasticity in the developing V1. It is well known that the maturation of inhibitory synapses in V1 is required for the onset of the critical period of OD plasticity.[1,26–29] Our finding thus supports the idea that the deficit in OD plasticity observed in astrocytic CB1R-deficient mice is caused by deficient maturation of inhibitory synapses affecting critical period onset.

During maturation of V1, inhibitory innervation changes extensively. During the first week after eye opening (p14–p21) the number and size of inhibitory synapses increase, resulting in stronger inhibition.[29] The causal link between inhibitory maturation and opening of the critical period of OD plasticity is well established. In mice with reduced GABA-release due to the absence of GAD65, a protein involved in GABA synthesis, the critical period does not start.[26,27] Increasing GABAergic transmission in these mice by intraventricular benzodiazepine infusion rescues the phenotype and initiates the critical period.[26] Furthermore, rearing animals in the dark, which extends the critical period for OD plasticity, delays the maturation of inhibitory synaptic transmission.[4,10,30] In addition to the general increase in synaptic strength, synaptic release and short-term depression decrease with development, resulting in more reliable and precise inhibition.[30–32] At inhibitory synapses formed by parvalbumin-expressing fast-spiking interneurons, the full maturation of inhibitory synaptic strength and dynamics depends on CB1R signaling, since both processes are disturbed by CB1R antagonist treatment or by genetic CB1R knockout.[3,4,10] This has been puzzling, since parvalbumin-expressing interneurons express no or only low levels of CB1Rs.[11–13] Our finding that inhibitory synaptic transmission undergoes normal maturation upon interneuron CB1R removal, but that maturation is affected when astrocyte CB1Rs are removed, provides an explanation for this apparent discrepancy.

The mechanism underlying CB1R-mediated inhibitory synapse maturation is not fully understood. In previous studies, CB1R inactivation resulted in both a blockade of iLTD and interference with inhibitory synapse maturation. Therefore, these processes were considered to be causally related.[3,4] Our study shows that the CB1Rs involved in inhibitory maturation are present on astrocytes. The observation that inhibitory synapse maturation is disturbed in GLAST-CB1R-KO mice, while iLTD is still intact, is surprising. This suggests that iLTD and inhibitory synaptic maturation are independent processes. But even in that scenario it would be expected that iLTD is reduced in one of the two conditional CB1R knockout lines. There are several potential explanations for this observation.

First, incomplete cell-type-specific CB1R deletion in GLAST-CB1R-KO mice may underlie the discrepancy. CB1R expression on a small percentage of cells may not support effective inhibitory maturation *in vivo* but might suffice to support iLTD expression *in vitro*. Recombination in GLAST-CB1R-KO mice is incomplete, which means that there will be CB1R expression in some astrocytes. The efficiency of recombination in the GLAST-CreERT2 line depends on a convergence of CreERT2 expression, local availability of 4OH-tamoxifen, and effective recombination. Experiments with TdTomato reporter mice (Figure 1) reveal reporter allele recombination in ~80% of astrocytes in V1 upon a single early postnatal tamoxifen injection. As full genetic CB1R removal from a cell requires bi-allelic recombination, we expect full CB1R removal in less than 80% of astrocytes.

iLTD induced in an acute brain slice by strong electrophysiological stimulation of a large number of inhibitory synapses might be more resilient to such incomplete CB1R inactivation than the physiological synaptic maturation process that alters inhibitory synaptic dynamics during development. Repeating the experiments described here using a constitutive astrocyte Cre driver line, such as an mGFAP-Cre line,[33] might yield a more complete knockout. But these lines show significant recombination in neural progenitors, which complicates interpretation of results.

Second, we cannot exclude that having CB1Rs on either astrocytes or interneurons suffices for iLTD induction or that it relies on CB1Rs on an additional cell type not targeted in our Cre-driver lines. Staining for the CB1R shows that although the majority of CB1R protein in visual cortex is found on inhibitory boutons, it is also expressed at excitatory boutons at substantially lower levels.[34] Detection of CB1R expression on astrocytes using standard microscopy is notoriously difficult because expression levels are low and the subcellular astrocyte specializations that contain the receptor are below the diffraction limit.[35,36] Importantly, the level of expression of the receptor at a certain location does not correlate with its functional relevance. Therefore, it would be very interesting to study the contribution of CB1R in, for example, excitatory neurons to *in vitro* and *in vivo* plasticity of inhibitory synapses in the mouse visual cortex using a similar approach as taken here.

Previous work has shown that pharmacological blockade of CB1Rs during monocular deprivation reduces OD plasticity. As this intervention does not interfere with CB1R signaling during development, it leaves inhibitory maturation intact. In these studies, OD plasticity was only affected in the superficial layers, whereas an OD shift could still be induced in layers 4–6.[24,25] LTD of excitatory synapses in L2/3 of sensory cortex is dependent on CB1Rs, whereas excitatory LTD (eLTD) in deeper layers is CB1R independent.[37,38] It is therefore believed that the effect of CB1R blockade during monocular deprivation is caused by selective and acute interference with eLTD in L2/3. We find that in astrocytic CB1R-deficient animals, OD plasticity is reduced in all layers of V1. This suggests that CB1Rs regulate OD plasticity through multiple mechanisms: acutely by mediating LTD at excitatory synapses in L2/3 neurons during monocular deprivation and developmentally by driving the development of inhibitory synapses throughout the cortex.[3] It was recently shown that in mice deficient for DGLα, essential for 2-AG synthesis, OD plasticity during the peak of the critical period was also reduced in all layers, matching our observations.[39] We do not know whether inactivating CB1Rs in astrocytes will also affect OD plasticity by an acute effect on excitatory LTD. But several studies have shown that astrocyte CB1Rs can regulate plasticity at excitatory synapses,[8] for instance by driving D-serine release necessary for NMDA receptor activation.[40] One would need to inactivate CB1Rs in astrocytes at a later age to dissociate developmental and acute astrocyte CB1R effects.

In GLAST-CB1R-KO mice, astrocyte CB1Rs are inactivated not only in V1 but also in the rest of the brain. We can therefore not rule out that the observed reduction of OD plasticity is caused by the absence of astrocytic CB1Rs in other brain structures, such as the dorsal lateral geniculate nucleus (dLGN) providing input to V1. We have shown that OD plasticity also occurs in the thalamus and that thalamic synaptic inhibition is essential for OD plasticity both in dLGN and in V1.[41] However, in the absence of thalamic inhibition, OD plasticity was predominantly affected after 7 days of MD, whereas after 3 days of MD, the OD shift was barely reduced.[41] In our current study, we saw a strong decrease of OD plasticity already after 3 days of MD in GLAST-CB1R mice, suggesting that reduced thalamic inhibition is not the main cause of this plasticity deficit.

Endocannabinoid signaling plays a role in maturation inhibitory synaptic transmission in the visual cortex and beyond,[42] but the direction and mechanisms are not fully understood and might show layer-, brain-region-, and temporal differences. A recent study showed that mice lacking the endocannabinoid synthesizing enzyme DGLα have an increased frequency of inhibitory miniature postsynaptic currents in L2/3 and L4 of V1 early during the second and third week of development, whereas they are decreased in L2/3 during the critical period.[39] In prefrontal cortex (PFC), activation of CB1Rs during development using the synthetic CB1R agonist WIN55,212-2 seems to impair inhibitory maturation.[43] Therefore, CB1R signaling may play opposite roles in inhibitory synapse maturation, depending on cortical layer, brain region, or developmental stage. Whether this depends on CB1Rs on different cell types is an exciting open question.

Our findings add to a larger body of research that reveals a role for astrocytes in regulating critical periods in the brain.[44,45] Interestingly, transplanting astrocytes from kittens into V1 of adult cats reopens the critical period of OD plasticity.[46] A more recent study found that transplanting immature astrocytes in V1 of adult mice reopens the critical period through degradation of the extracellular matrix.[45] We hypothesize that CB1Rs on astrocytes contribute to critical period regulation through a different mechanism: stimulating inhibitory synapse maturation. It thus seems unlikely that CB1Rs will contribute to the reopening of the critical period in adult V1 by immature astrocytes, as by then inhibitory synapses have already reached maturity. Together these studies show that understanding critical period plasticity requires taking the interactions between neurons and glial cells into account.

Limitations of the study

Here, we studied the role of astrocyte CB1Rs in the development of inhibitory synapses and OD plasticity in V1. For this purpose, we inactivated the *Cnr1* gene in astrocytes by making use of mice in which the CB1R gene was flanked by loxP-sites and that were carrying a GLAST-CreERT2 transgene. One limitation of this study is that CB1R expression was not lost in all cortical astrocytes, possibly causing an incomplete phenotype. Another limitation is that CB1 inactivation was not limited to V1, where we assessed inhibitory maturation and OD plasticity, potentially also causing plasticity deficits in other brain regions.

RESOURCE AVAILABILITY

Lead contact

Further information and requests for resources and reagents should be directed to and will be fulfilled by the lead contact, Christiaan Levelt (c.levelt@nin.knaw.nl).

Materials availability

This study did not generate new unique reagents.

Data and code availability

Processed data for reproducing figures and/or analysis reported in this manuscript have been deposited at Figshare (https://doi.org/10.6084/m9.figshare.27309591) and are publicly available as of the date of publication. Accession numbers are listed in the key resources table. Any additional information required to reanalyze the data reported in this paper is available from the lead contact upon request.

ACKNOWLEDGMENTS

The authors thank Giovanni Marsicano (Inserm, Bordeaux, France) and Beat Lutz (University Medical Center of the Johannes Gutenberg University, Mainz, Germany) for providing *Cnr1*$^{flox/flox}$ mice, Emma Ruimschotel (NIN, Amsterdam, the Netherlands) for excellent technical assistance, and Alexander Heimel (NIN, Amsterdam, the Netherlands) for valuable discussions. This study was funded by an NWO Veni grant to R.M. (863.12.006).

AUTHOR CONTRIBUTIONS

Conceptualization: R.M. and C.N.L.; investigation: R.M., Y.Q., S.K., M.H.S., and M.v.L.; formal analysis: R.M., Y.Q., and S.K.; visualization: R.M.; writing—original draft: R.M. and C.N.L.; writing—review & editing: R.M. and C.N.L.; supervision: C.N.L.; funding acquisition: R.M. and C.N.L.

DECLARATION OF INTERESTS

The authors declare no competing interests.

STAR★METHODS

Detailed methods are provided in the online version of this paper and include the following:

- KEY RESOURCES TABLE
- EXPERIMENTAL MODEL AND STUDY PARTICIPANT DETAILS
- METHOD DETAILS
  - Tamoxifen injection
  - Monocular deprivation
  - Intrinsic signal imaging/electrophysiology
  - Slice electrophysiology
  - Immunohistochemistry
- QUANTIFICATION AND STATISTICAL ANALYSIS

SUPPLEMENTAL INFORMATION

Supplemental information can be found online at https://doi.org/10.1016/j.isci.2024.111410.

Received: December 20, 2023
Revised: October 2, 2024
Accepted: November 13, 2024
Published: November 17, 2024

REFERENCES

1. Hensch, T.K. (2005). Critical period plasticity in local cortical circuits. Nat. Rev. Neurosci. *6*, 877–888. https://doi.org/10.1038/nrn1787.
2. Chevaleyre, V., Takahashi, K.A., and Castillo, P.E. (2006). Endocannabinoid-mediated synaptic plasticity in the CNS. Annu. Rev. Neurosci. *29*, 37–76. https://doi.org/10.1146/annurev.neuro.29.051605.112834.
3. Sun, W., Wang, L., Li, S., Tie, X., and Jiang, B. (2015). Layer-specific endocannabinoid-mediated long-term depression of GABAergic neurotransmission onto principal neurons in mouse visual cortex. Eur. J. Neurosci. *42*, 1952–1965. https://doi.org/10.1111/ejn.12958.
4. Jiang, B., Huang, S., de Pasquale, R., Millman, D., Song, L., Lee, H.K., Tsumoto, T., and Kirkwood, A. (2010). The maturation of GABAergic transmission in visual cortex requires endocannabinoid-mediated LTD of inhibitory inputs during a critical period. Neuron *66*, 248–259. https://doi.org/10.1016/j.neuron.2010.03.021.
5. Gordon, J.A., and Stryker, M.P. (1996). Experience-dependent plasticity of binocular responses in the primary visual cortex of the mouse. J. Neurosci. *16*, 3274–3286. https://doi.org/10.1523/JNEUROSCI.16-10-03274.1996.
6. Cynader, M., and Mitchell, D.E. (1980). Prolonged sensitivity to monocular deprivation in dark-reared cats. J. Neurophysiol. *43*, 1026–1040. https://doi.org/10.1152/jn.1980.43.4.1026.
7. Navarrete, M., and Araque, A. (2008). Endocannabinoids mediate neuron-astrocyte communication. Neuron *57*, 883–893. https://doi.org/10.1016/j.neuron.2008.01.029.
8. Min, R., and Nevian, T. (2012). Astrocyte signaling controls spike timing-dependent depression at neocortical synapses. Nat. Neurosci. *15*, 746–753. https://doi.org/10.1038/nn.3075.
9. Han, J., Kesner, P., Metna-Laurent, M., Duan, T., Xu, L., Georges, F., Koehl, M., Abrous, D.N., Mendizabal-Zubiaga, J., Grandes, P., et al. (2012). Acute cannabinoids impair working memory through astroglial CB1 receptor modulation of hippocampal LTD. Cell *148*, 1039–1050. https://doi.org/10.1016/j.cell.2012.01.037.
10. Huang, S., and Kirkwood, A. (2020). Endocannabinoid Signaling Contributes to Experience-Induced Increase of Synaptic Release Sites From Parvalbumin Interneurons in Mouse Visual Cortex. Front. Cell. Neurosci. *14*, 571133. https://doi.org/10.3389/fncel.2020.571133.
11. Hill, E.L., Gallopin, T., Férézou, I., Cauli, B., Rossier, J., Schweitzer, P., and Lambolez, B. (2007). Functional CB1 receptors are broadly expressed in neocortical GABAergic and glutamatergic neurons. J. Neurophysiol. *97*, 2580–2589. https://doi.org/10.1152/jn.00603.2006.
12. Wedzony, K., and Chocyk, A. (2009). Cannabinoid CB1 receptors in rat medial prefrontal cortex are colocalized with calbindin- but not parvalbumin- and calretinin-positive GABA-ergic neurons. Pharmacol. Rep. *61*, 1000–1007. https://doi.org/10.1016/s1734-1140(09)70161-6.
13. Bodor, A.L., Katona, I., Nyíri, G., Mackie, K., Ledent, C., Hájos, N., and Freund, T.F. (2005). Endocannabinoid signaling in rat somatosensory cortex: laminar differences and involvement of specific interneuron types. J. Neurosci. *25*, 6845–6856. https://doi.org/10.1523/JNEUROSCI.0442-05.2005.
14. Marsicano, G., Goodenough, S., Monory, K., Hermann, H., Eder, M., Cannich, A., Azad, S.C., Cascio, M.G., Gutiérrez, S.O., van der Stelt, M., et al. (2003). CB1 cannabinoid receptors and on-demand defense against excitotoxicity. Science *302*, 84–88. https://doi.org/10.1126/science.1088208.
15. Taniguchi, H., He, M., Wu, P., Kim, S., Paik, R., Sugino, K., Kvitsiani, D., Fu, Y., Lu, J., Lin, Y., et al. (2011). A resource of Cre driver lines for genetic targeting of GABAergic neurons in cerebral cortex. Neuron *71*, 995–1013. https://doi.org/10.1016/j.neuron.2011.07.026.
16. Wang, Y., Rattner, A., Zhou, Y., Williams, J., Smallwood, P.M., and Nathans, J. (2012). Norrin/Frizzled4 signaling in retinal vascular development and blood brain barrier plasticity. Cell *151*, 1332–1344. https://doi.org/10.1016/j.cell.2012.10.042.
17. Srinivasan, R., Lu, T.Y., Chai, H., Xu, J., Huang, B.S., Golshani, P., Coppola, G., and Khakh, B.S. (2016). New Transgenic Mouse Lines for Selectively Targeting Astrocytes and Studying Calcium Signals in Astrocyte Processes In Situ and In Vivo. Neuron *92*, 1181–1195. https://doi.org/10.1016/j.neuron.2016.11.030.
18. Cheli, V.T., Santiago González, D.A., Wan, Q., Denaroso, G., Wan, R., Rosenblum, S.L., and Paez, P.M. (2021). H-ferritin expression in astrocytes is necessary for proper oligodendrocyte development and myelination. Glia *69*, 2981–2998. https://doi.org/10.1002/glia.24083.
19. Cheli, V.T., Sekhar, M., Santiago González, D.A., Angeliu, C.G., Denaroso, G.E., Smith, Z., Wang, C., and Paez, P.M. (2023). The expression of ceruloplasmin in astrocytes is essential for postnatal myelination and myelin maintenance in the adult brain. Glia *71*, 2323–2342. https://doi.org/10.1002/glia.24424.

20. Higashimori, H., Schin, C.S., Chiang, M.S.R., Morel, L., Shoneye, T.A., Nelson, D.L., and Yang, Y. (2016). Selective Deletion of Astroglial FMRP Dysregulates Glutamate Transporter GLT1 and Contributes to Fragile X Syndrome Phenotypes In Vivo. J. Neurosci. *36*, 7079–7094. https://doi.org/10.1523/JNEUROSCI.1069-16.2016.

21. Heimel, J.A., Hartman, R.J., Hermans, J.M., and Levelt, C.N. (2007). Screening mouse vision with intrinsic signal optical imaging. Eur. J. Neurosci. *25*, 795–804. https://doi.org/10.1111/j.1460-9568.2007.05333.x.

22. Frostig, R.D., Masino, S.A., Kwon, M.C., and Chen, C.H. (1995). Using light to probe the brain: Intrinsic signal optical imaging. Int. J. Imaging Syst. Technol. *6*, 216–224. https://doi.org/10.1002/ima.1850060212.

23. Masino, S.A. (2003). Quantitative comparison between functional imaging and single-unit spiking in rat somatosensory cortex. J. Neurophysiol. *89*, 1702–1712. https://doi.org/10.1152/jn.00860.2002.

24. Liu, C.H., Heynen, A.J., Shuler, M.G.H., and Bear, M.F. (2008). Cannabinoid receptor blockade reveals parallel plasticity mechanisms in different layers of mouse visual cortex. Neuron *58*, 340–345.

25. Frantz, M.G., Crouse, E.C., Sokhadze, G., Ikrar, T., Stephany, C.É., Nguyen, C., Xu, X., and McGee, A.W. (2020). Layer 4 Gates Plasticity in Visual Cortex Independent of a Canonical Microcircuit. Curr. Biol. *30*, 2962–2973.e5. https://doi.org/10.1016/j.cub.2020.05.067.

26. Fagiolini, M., and Hensch, T.K. (2000). Inhibitory threshold for critical-period activation in primary visual cortex. Nature *404*, 183–186. https://doi.org/10.1038/35004582.

27. Hensch, T.K., Fagiolini, M., Mataga, N., Stryker, M.P., Baekkeskov, S., and Kash, S.F. (1998). Local GABA circuit control of experience-dependent plasticity in developing visual cortex. Science *282*, 1504–1508. https://doi.org/10.1126/science.282.5393.1504.

28. Hanover, J.L., Huang, Z.J., Tonegawa, S., and Stryker, M.P. (1999). Brain-derived neurotrophic factor overexpression induces precocious critical period in mouse visual cortex. J. Neurosci. *19*, RC40. https://doi.org/10.1523/JNEUROSCI.19-22-j0003.1999.

29. Huang, Z.J., Kirkwood, A., Pizzorusso, T., Porciatti, V., Morales, B., Bear, M.F., Maffei, L., and Tonegawa, S. (1999). BDNF regulates the maturation of inhibition and the critical period of plasticity in mouse visual cortex. Cell *98*, 739–755. https://doi.org/10.1016/s0092-8674(00)81509-3.

30. Morales, B., Choi, S.Y., and Kirkwood, A. (2002). Dark rearing alters the development of GABAergic transmission in visual cortex. J. Neurosci. *22*, 8084–8090. https://doi.org/10.1523/JNEUROSCI.22-18-08084.2002.

31. Jiang, B., Huang, Z.J., Morales, B., and Kirkwood, A. (2005). Maturation of GABAergic transmission and the timing of plasticity in visual cortex. Brain Res. Brain Res. Rev. *50*, 126–133. https://doi.org/10.1016/j.brainresrev.2005.05.007.

32. Tang, A.H., Chai, Z., and Wang, S.Q. (2007). Dark rearing alters the short-term synaptic plasticity in visual cortex. Neurosci. Lett. *422*, 49–53. https://doi.org/10.1016/j.neulet.2007.05.053.

33. Gregorian, C., Nakashima, J., Le Belle, J., Ohab, J., Kim, R., Liu, A., Smith, K.B., Groszer, M., Garcia, A.D., Sofroniew, M.V., et al. (2009). Pten deletion in adult neural stem/progenitor cells enhances constitutive neurogenesis. J. Neurosci. *29*, 1874–1886. https://doi.org/10.1523/JNEUROSCI.3095-08.2009.

34. Yoneda, T., Kameyama, K., Esumi, K., Daimyo, Y., Watanabe, M., and Hata, Y. (2013). Developmental and visual input-dependent regulation of the CB1 cannabinoid receptor in the mouse visual cortex. PLoS One *8*, e53082. https://doi.org/10.1371/journal.pone.0053082.

35. Achicallende, S., Bonilla-Del Río, I., Serrano, M., Mimenza, A., Lekunberri, L., Anaut-Lusar, I., Puente, N., Gerrikagoitia, I., and Grandes, P. (2022). GLAST versus GFAP as astroglial marker for the subcellular study of cannabinoid CB(1) receptors in astrocytes. Histochem. Cell Biol. *158*, 561–569. https://doi.org/10.1007/s00418-022-02139-4.

36. Puente, N., Río, I.B.D., Achicallende, S., Nahirney, P.C., and Grandes, P. (2019). High-resolution Immunoelectron Microscopy Techniques for Revealing Distinct Subcellular Type 1 Cannabinoid Receptor Domains in Brain. Bio. Protoc. *9*, e3145. https://doi.org/10.21769/BioProtoc.3145.

37. Crozier, R.A., Wang, Y., Liu, C.H., and Bear, M.F. (2007). Deprivation-induced synaptic depression by distinct mechanisms in different layers of mouse visual cortex. Proc. Natl. Acad. Sci. USA *104*, 1383–1388. https://doi.org/10.1073/pnas.0609596104.

38. Banerjee, A., Meredith, R.M., Rodríguez-Moreno, A., Mierau, S.B., Auberson, Y.P., and Paulsen, O. (2009). Double dissociation of spike timing-dependent potentiation and depression by subunit-preferring NMDA receptor antagonists in mouse barrel cortex. Cereb. Cortex *19*, 2959–2969. https://doi.org/10.1093/cercor/bhp067.

39. Yoneda, T., Kameyama, K., Gotou, T., Terata, K., Takagi, M., Yoshimura, Y., Sakimura, K., Kano, M., and Hata, Y. (2024). Layer specific regulation of critical period timing and maturation of mouse visual cortex by endocannabinoids. iScience *27*, 110145. https://doi.org/10.1016/j.isci.2024.110145.

40. Robin, L.M., Oliveira da Cruz, J.F., Langlais, V.C., Martin-Fernandez, M., Metna-Laurent, M., Busquets-Garcia, A., Bellocchio, L., Soria-Gomez, E., Papouin, T., Varilh, M., et al. (2018). Astroglial CB1 Receptors Determine Synaptic D-Serine Availability to Enable Recognition Memory. Neuron *98*, 935–944.e5. https://doi.org/10.1016/j.neuron.2018.04.034.

41. Sommeijer, J.P., Ahmadlou, M., Saiepour, M.H., Seignette, K., Min, R., Heimel, J.A., and Levelt, C.N. (2017). Thalamic inhibition regulates critical-period plasticity in visual cortex and thalamus. Nat. Neurosci. *20*, 1715–1721. https://doi.org/10.1038/s41593-017-0002-3.

42. Younts, T.J., and Castillo, P.E. (2014). Endogenous cannabinoid signaling at inhibitory interneurons. Curr. Opin. Neurobiol. *26*, 42–50. https://doi.org/10.1016/j.conb.2013.12.006.

43. Cass, D.K., Flores-Barrera, E., Thomases, D.R., Vital, W.F., Caballero, A., and Tseng, K.Y. (2014). CB1 cannabinoid receptor stimulation during adolescence impairs the maturation of GABA function in the adult rat prefrontal cortex. Mol. Psychiatry *19*, 536–543. https://doi.org/10.1038/mp.2014.14.

44. Ackerman, S.D., Perez-Catalan, N.A., Freeman, M.R., and Doe, C.Q. (2021). Astrocytes close a motor circuit critical period. Nature *592*, 414–420. https://doi.org/10.1038/s41586-021-03441-2.

45. Ribot, J., Breton, R., Calvo, C.F., Moulard, J., Ezan, P., Zapata, J., Samama, K., Moreau, M., Bemelmans, A.P., Sabatet, V., et al. (2021). Astrocytes close the mouse critical period for visual plasticity. Science *373*, 77–81. https://doi.org/10.1126/science.abf5273.

46. Müller, C.M., and Best, J. (1989). Ocular dominance plasticity in adult cat visual cortex after transplantation of cultured astrocytes. Nature *342*, 427–430. https://doi.org/10.1038/342427a0.

47. Madisen, L., Zwingman, T.A., Sunkin, S.M., Oh, S.W., Zariwala, H.A., Gu, H., Ng, L.L., Palmiter, R.D., Hawrylycz, M.J., Jones, A.R., et al. (2010). A robust and high-throughput Cre reporting and characterization system for the whole mouse brain. Nat. Neurosci. *13*, 133–140. https://doi.org/10.1038/nn.2467.

48. Brainard, D.H. (1997). The Psychophysics Toolbox. Spat. Vis. *10*, 433–436.

STAR★METHODS

KEY RESOURCES TABLE

REAGENT or RESOURCE	SOURCE	IDENTIFIER
Antibodies		
Glutamine Synthetase (monoclonal mouse)	Merck Millipore	MAB302; RRID: AB_2110656
NeuN (monoclonal mouse)	Merck Millipore	MAB377; RRID: AB_2298767
NG2 (polyclonal rabbit)	Merck Millipore	AB5320; RRID: AB_91789
Olig2 (monoclonal mouse)	Merck Millipore	MABN50; RRID: AB_10807410
Chemicals, peptides, and recombinant proteins		
Tamoxifen	Sigma-Aldrich	T5648
Corn Oil	Sigma-Aldrich	C8267
Isoflurane	Zoetis Isoflo	REG NL 10416 UDD
Cavasan eye ointment	AST Farma	REG NL 4006
Deposited data		
Processed data for reproducing figures and/or analysis	This manuscript	figshare: https://doi.org/10.6084/m9.figshare.27309591
Experimental models: Organisms/strains		
Mouse: *Cnr1*$^{flox/flox}$	Marsicano et al.[14]	N/A
Mouse: Gad2-IRES-Cre	Jackson Laboratory	Jax Stock No: 019022
Mouse: GLAST-CreERT2	Jackson Laboratory	Jax Stock No: 012586
Mouse: ROSA-TdTomato reporter	Jackson Laboratory	Jax Stock No: 007908
Software and algorithms		
MATLAB	MathWorks	https://www.mathworks.com/products/matlab.html
Invivotools, custom-written code	Heimel/Levelt lab	http://github.com/heimel/inVivoTools
PClamp software	Molecular Devices	www.moleculardevices.com/
IGOR Pro	WaveMetrics	https://www.wavemetrics.com/
GraphPad Prism	GraphPad Software	https://www.graphpad.com/

EXPERIMENTAL MODEL AND STUDY PARTICIPANT DETAILS

Experimental procedures involving mice were in strict compliance with animal welfare policies of the Dutch government and were approved by the Institutional Animal Care and Use Committee of the Netherlands Institute for Neuroscience. (License numbers: AVD8010020171045 and AVD80100202215934). Genetically-modified mice were bred on a C57Bl6/J background. For generation of conditional CB1R knockout mice, mice homozygous for a loxP-site flanked CB1R gene (*Cnr1*$^{flox/flox}$ mice)[14] and heterozygous for either GAD2-Cre (Gad2-IRES-Cre mice; Jax Stock No: 019022)[15] or GLAST-CreERT2 (Jax Stock No: 012586) were bred with mice homozygous for *Cnr1*$^{flox/flox}$ without either of the Cre alleles. Offspring was therefore homozygous for *Cnr1*$^{flox/flox}$ and either wild-type or heterozygous for a Cre allele. To assess efficacy and specificity of recombination in GLAST-CreERT2 mice, these mice were crossed with ROSA-TdTomato reporter mice,[47] in which a Cre-dependent transgene encoding the tdTomato fluorescent protein is inserted in the ROSA26 locus (Jax Stock No: 007908). Experiments were performed on mice of either sex. Age of used mice varied with the experiment and is specified in the relevant results section. Animals were housed on a 12 h light/dark cycle with unlimited access to standard lab chow and water.

METHOD DETAILS

Tamoxifen injection

Mouse pups received a single intraperitoneal (i.p.) tamoxifen injection to induce Cre mediated recombination in the GLAST-CreERT2 line. Tamoxifen was dissolved in corn oil at a final concentration of 5 mg/mL. Dissolving tamoxifen was aided by placing the Eppendorf tube in an ultrasonic water bath, heated to 30°C, for ~1 h. Tamoxifen solution (25 μL) was injected using a thin insulin needle. To assess specificity and efficacy of recombination injections were performed either at P1 or between P3-P5. For all further experiments a single injection between P3-P5 was used.

Monocular deprivation

Surgery for monocular deprivation (MD) was performed as follows: Mice were anesthetized using isoflurane (5% induction, 1.5–2% maintenance in 0.7 L/min O2). Edges of the upper and lower eyelids of the right eye (contralateral to the side on which recordings were performed) were carefully removed. Antibiotic ointment (Cavasan) was applied. Eyelids were sutured together with 2–3 sutures using 7.0 Ethilon thread during isoflurane anesthesia. Postoperative lidocaine ointment was applied to the closed eyelid. Eyes were checked for infection or opacity once reopened 3 days later, and only mice with clear corneas were included.

Intrinsic signal imaging/electrophysiology

Mice were anesthetized by intraperitoneal injection of urethane (20% solution in saline, 1.2 g/kg body weight), supplemented by a subcutaneous injection of chlorprothixene (2.0 mg/mL in saline, 8 mg/kg body weight). Sometimes a supplement of about 10% of the original dose of urethane was necessary. Injection of anesthetic was immediately followed by a subcutaneous injection of atropine sulfate (50 μg/mL in saline, 1 μg/10g body weight) to reduce secretions from mucous membranes and facilitate breathing. Anesthesia reached sufficient depth after 45–60 min. Body temperature was monitored with a rectal probe and maintained at a temperature at 36.5°C using a heating pad. The animal was fixated by ear bars with conical tips prepared with lidocaine ointment. A bite rod was positioned behind the front teeth, 4 mm lower than the ear bars. A continuous flow of oxygen was provided close to the nose. For analgesia of the scalp, xylocaine ointment (lidocaine HCl) was applied before resection of a part of the scalp to expose the skull.

OD measurements were performed as previously described.[21] In brief, the exposed skull was illuminated with 700 ± 30 nm light and the intensity of reflected light was measured. Responses were acquired with an Imager 3001 system (Optical Imaging, Israel). A gamma corrected computer screen was placed in front of the mouse, covering an area of the mouse visual field ranging from −15 to 75° horizontally and −45 to 45° vertically. First the retinotopic representation of V1 was mapped. Full contrast, square wave gratings of 0.05 cycles per degree (cpd), moving at 2 Hz and changing direction every 0.6 s were shown every 9 s for 3 s in a pseudo-randomly chosen quadrant while the rest of the screen was a constant gray. Fifteen stimuli in each quadrant were sufficient to construct a robust retinotopic map of V1. To subsequently measure OD, shutters were placed in front of both eyes. Either shutter opened independently at preset intervals, for a period of 6 s. After full opening of the shutter, the visual stimuli described above were presented in the upper nasal quadrant of the screen for a period of 3 s. Fifty responses to stimulation were recorded for each eye. For quantification, the response of a defined region of interest within the binocular part of V1 (as determined by retinotopic mapping) was normalized to the response seen in a region of reference (ROR) outside of V1, which lacked a stimulus specific response. The negative ratio of ROI over ROR signal was taken, normalized to the stimulus onset and averaged from the first frame after stimulus onset until 2s after stimulus offset. The Ocular Dominance Index (ODI) was calculated as (contralateral response − ipsilateral response)/(contralateral response + ipsilateral response).

For *in vivo* electrophysiology, a craniotomy was prepared over V1, 2.95 mm lateral and 0.45 mm anterior to lambda. Mice were placed in front of a gamma-corrected projector (PLUS U2-X1130 DLP), which projected visual stimuli onto a back-projection screen (Macada Innovision, the Netherlands; 60 × 42 cm area) positioned 17.5 cm in front of the mouse. One eye was covered with a double layer of black fabric and black tape while neuronal responses to stimulation of the other eye were recorded. Visual stimuli were created with the MATLAB (MathWorks) software package Psychophysics Toolbox 3.[48] The position of the receptive field was determined by displaying white squares (5°) at random locations on a black background. The ODI was calculated by presenting each eye with alternating white and gray full-screen stimuli. Each stimulation lasted 3 s. There were 100 repetitions of both white and gray screens. Extracellular recordings from V1 were made using a linear silicon microelectrode (A1x16-5mm-25-177-A16, 16 channels spaced 50 m apart, Neuronexus, USA). Extracellular signals were amplified and bandpass filtered at 500 Hz-10 kHz before being digitized at 24 kHz using an RX5 Pentusa base station (Tucker-Davis Technologies, USA). A voltage thresholder at 3x standard deviation was used to detect spikes online. Custom-written MATLAB programs (http://github.com/heimel/inVivoTools) were used to analyze the data. We computed the spike - triggered average of the random spare square stimulus for receptive field mapping. The actual position and size of the visual field were calculated and corrected for the distance between the stimulus and the animal. We used the last 500ms of the previous trail as the baseline for each 3 s stimulus-related activity. As a result, we characterized visual responses as the difference between the first 500ms of the stimulus and the mean of the prior stimulus's last 500ms activities. The greatest firing rates in the first 300ms of visual related reactions were regarded the peak visual responses to stimuli. The visual responses were calculated as 300ms average multi-unit responses. ODI was calculated as $(R_{contra} - R_{ipsi})/(R_{contra} + R_{ipsi})$, where the R_{contra} is the average multi-unit firing rate of the unit when contralateral eye was open and ipsilateral eye was covered; R_{ipsi} is opposite.

Slice electrophysiology

For acute brain slice preparation, animals aged between P14-35 were briefly anesthetized using isoflurane, followed by decapitation. Brains were removed and placed in ice-cold slicing medium. For most experiments sucrose based slicing medium was used, containing (in mM): 212.7 sucrose, 26 NaHCO3, 3 KCl, 1.25 NaH2PO4, 1 CaCl2, 3 MgCl2 and 10 D(+)-glucose (carbogenated with 5% CO2/95% O2; osmolarity 300–310 mOsm). For some experiments choline chloride based slicing medium, containing (in mM): 110 choline chloride, 7 MgCl2, 0.5 CaCl2, 2.5 KCl, 11.6 Na-ascorbate, 3.10 Na-pyruvate, 1.25 NaH2PO4, 25 D-glucose and 25 NaHCO3 (carbogenated with 5% CO2/95% O2; osmolarity 300–310 mOsm) was used. Quality of slices and properties of recorded neurons were indistinguishable for both solutions. Coronal slices (350 μm) containing V1 were prepared using a vibratome. Within

each slice, the hemispheres were separated with a scalpel at the middle axis to be used for individual recordings. The slices were transferred to a holding chamber and left to recover for at least 30 min at 35°C in carbogenated artificial cerebrospinal fluid (ACSF), containing (mM): 124 NaCl, 26 NaHCO3, 3 KCl, 1.25 NaH2PO4, 2 CaCl2, 1 MgCl2 and 10 D(+)-glucose (carbogenated with 5% CO2/95% O2; osmolarity 300–310 mOsm). After recovery the holding chamber was moved to room temperature and slices were kept until recording (up to 8 h after slice preparation).

For recording, slices were transferred to the stage of an upright microscope, where they were continuously perfused with heated (30°C–32°C) ACSF. NMDA receptor and AMPA receptor mediated glutamatergic synaptic responses were blocked by addition of D-AP5 (50 μM) and DNQX (10 μM) to the recording ACSF. Whole cell patch-clamp recordings from pyramidal neurons in Layer 2/3 of V1 were made using a Multiclamp 700B amplifier in voltage clamp mode and PClamp software (Molecular Devices, USA). Cells were patched with borosilicate glass electrodes with tip resistances of ∼3.5 MOhm, and filled with intracellular solution containing (mM): 120 CsCl, 8 NaCl, 10 HEPES, 2 EGTA, 10 Na-phosphocreatine, 4 Mg-ATP, 0.5 Na-GTP and 5 QX-314 (pH: 7.4; osmolarity ∼285 mOsm). IPSCs were evoked with an ACSF filled glass electrode with a broken tip or with a concentric bipolar stimulation electrode, placed in Layer 4. Intensity of the stimulation pulse was adjusted to obtain a reliable and stable IPSC response.

For experiments in which iLTD was evoked, IPSCs were evoked every 20 s until a stable baseline was established. Next, iLTD was induced using theta-burst stimulation (TBS), consisting of 8–10 thetaburst epochs delivered every 5 s. Each theta-burst epoch consisted of 10 trains of 5 pulses at 100 Hz, with the trains being delivered at 5 Hz (adapted from[3,4]). In a small subset of experiments, the strength of extracellular stimulation was doubled during TBS delivery. Because this did not affect the magnitude or dynamics of iLTD, all experiments were grouped for final analysis. AM251 was diluted in DMSO, and the stock solution was added to ACSF to obtain a final concentration of 10 μM (final DMSO concentration: 0.1%).

IPSC amplitude was analyzed using custom scripts in IGOR pro (WaveMetrics, USA). For iLTD analysis, magnitude of iLTD was determined by comparing the IPSC amplitude during the 10 min baseline to the IPSC amplitude 10–20 min after TBS. Recordings were excluded if the IPSC amplitude differed >12.5% between the first and the last 6 responses of the baseline, if input resistance increased >25% between baseline and iLTD window, if access resistance increased to >20 MOhm, or if leak current reached lower than −500 pA.

Immunohistochemistry

Mice were anesthetized with an overdose of pentobarbital (100 mg/kg i.p.), followed by transcardial perfusion with 4% paraformaldehyde (PFA) in phosphate buffered saline (PBS). Brains were isolated and post-fixated for >2 h in PFA at 4°C. After changing to PBS, coronal slices (50 μm thickness) were prepared. Slices were incubated for 2 h in 500 μL blocking solution (0.1% Triton X-100, 5% NGS in PBS) on a rotary shaker at room temperature. Afterward, slices were incubated with primary antibody containing solution and left overnight at 4°. The next day primary antibody solution was discarded, and slices were washed three times for 10 min at room temperature on the rotary shaker with 500 μL of washing solution (0.1% Tween in PBS). Secondary antibody solution (250 μL) was added per well and slices were incubated for 1 h at room temperature on the rotary shaker. Next, slices were again washed three times for 10 min at room temperature on the rotary shaker with washing solution. Stained slices were mounted on glass slides using Mowiol. The following antibodies were used: Glutamine Synthetase (monoclonal mouse, MAB302, Merck Millipore, USA), NeuN (monoclonal mouse, 1:1000, MAB377, Merck Millipore, USA), NG2 (polyclonal rabbit, 1:250, AB5320, Merck Millipore, USA) and Olig2 (monoclonal mouse, 1:250, MABN50, Merck Millipore, USA). Secondary antibody conjugated with Alexa 488 was used (1:250 or 1:500, ThermoFisher, USA). Imaging of the immunostained sections was done using a Leica TCS SP5 Confocal microscope (Leica, Germany).

QUANTIFICATION AND STATISTICAL ANALYSIS

Data representation and statistical analysis were performed using GraphPad Prism 10.2.0 (GraphPad Software, USA). Parametric or non-parametric statistics were used depending on whether data points were normally distributed. When necessary, correction for multiple comparisons was applied (Tukey's post-hoc test for two-way ANOVA). The used tests are indicated in the text and all details of statistical analysis can be found in Table S1. The number of measurements is indicated using n, while the number of animals from which these measurements arise is indicated using N. Statistically significant differences were defined as $p \leq 0.05$. The following indicators are used in figures: *: $p \leq 0.05$; **: $p \leq 0.01$; ***: $p \leq 0.001$. Data are represented as mean ± SEM.